

## Current reversal and particle separation in Brownian transport

Hai-Wei Hu <sup>1,2</sup>, Lin Du <sup>1,2,\*</sup>, Liang-Hui Qu,<sup>1,2</sup> Zi-Lu Cao,<sup>1,2</sup> Zi-Chen Deng,<sup>1,2,3</sup> and Ying-Cheng Lai <sup>4,5</sup>

<sup>1</sup>*School of Mathematics and Statistics, Northwestern Polytechnical University, Xi'an 710072, China*

<sup>2</sup>*MIT Key Laboratory of Dynamics and Control of Complex Systems, Northwestern Polytechnical University, Xi'an 710072, China*

<sup>3</sup>*School of Aeronautics, Northwestern Polytechnical University, Xi'an 710072, China*

<sup>4</sup>*School of Electrical, Computer and Energy Engineering, Arizona State University, Tempe, Arizona 85287, USA*

<sup>5</sup>*Department of Physics, Arizona State University, Tempe, Arizona 85287, USA*



(Received 24 February 2021; accepted 19 July 2021; published 18 August 2021)

In transport of micro- or nanosized particles through a confined structure driven by thermal fluctuations and external forcing—a situation that arises commonly in a variety of fields in physical and biological sciences, efficient and controllable separation of particles of different sizes is an important but challenging problem. We study, numerically and analytically, the diffusion dynamics of Brownian particles through the biologically relevant setting of a spatially periodic structure, subject to static and temporally periodic forcing. Molecular dynamical simulations reveal that the mean velocity in general depends sensitively on the particle size. The phenomenon of current reversal is uncovered, where particles larger than or smaller than a critical size diffuse in exactly opposite directions. This striking behavior occurs in a wide range of the forcing amplitude and provides a mechanism to separate the Brownian particles of different sizes. Besides the forcing amplitude, other parametric quantities characterizing the forcing profile, such as the temporal asymmetry, can also be exploited to modulate or control the transport dynamics of particles of different sizes. To gain a theoretical understanding, we exploit the Fick-Jacobs approximation to obtain a one-dimensional description of the diffusion problem, which enables key quantities characterizing the diffusion process, such as the mean velocity, to be predicted. In the regime of weak forcing, a reasonable agreement between theory and numerical results is achieved. Beyond the weakly forcing regime, the diffusion approximation breaks down, causing the theoretical predictions to deviate from the numerical results, into which we provide physical insights. Our findings have potential applications in optimizing transport in microfluidic devices or through biological channels.

DOI: [10.1103/PhysRevResearch.3.033162](https://doi.org/10.1103/PhysRevResearch.3.033162)

### I. INTRODUCTION

In transport of micro- or nanosized particles through a confined space, e.g., a restricted channel, the influence of thermal fluctuations is predominant. The particles are thus Brownian particles and their diffusion and transport dynamics are relevant not only to traditional disciplines such as physics, chemistry, biology, engineering, and medicine, but also to recently emergent interdisciplinary fields such as nanotechnology and nanomedicine [1–9]. Restricted channels arise commonly in structures such as nanopores [10–12], zeolites [13,14], and ionic channels [15,16]. In nanomedicine, designing micro-nano scale channels for separating particles of different sizes is a fundamental problem [11]. The transport problem is also relevant to diverse problems such as microfluidics based drug screening [17], ion exchange in zeolite [13],

and potassium and sodium ions passing through ion channels as they enter and leave cells [15].

Historically, particle diffusion through a symmetric channel was studied theoretically using the concept of “entropy resistance” and the Fick-Jacobs type of diffusion equation [18,19]. It was found that the entropy resistance is related to the boundary conditions of the geometric structure in the confined space. Later, a modified Fick-Jacobs equation was derived [20], where the constant diffusion coefficient in the original Fick-Jacobs equation was replaced by a diffusion coefficient that depends on the boundary conditions stipulated by the geometric structure of the channel. The modification led to an equation governing the evolution of the probability density. The classic problem of particle diffusion through a periodically constrained structure was extended to a wider range of applications where, for example, the method of exploiting the entropy potential effect to manipulate particle motion was proposed [21]. In situations where the particles can achieve a rapid equilibrium in the cross-sectional degrees of freedom of the channel, the two-dimensional (2D) or three-dimensional (3D) diffusion problem can effectively be reduced to one in one dimension [22–25]. In particular, when the cross-sectional integration is removed because of the fast achieved equilibrium, the effective entropy barrier due to the limited space will appear in the diffusion equation. Using the concept of

\*lindu@nwpu.edu.cn

Published by the American Physical Society under the terms of the [Creative Commons Attribution 4.0 International license](https://creativecommons.org/licenses/by/4.0/). Further distribution of this work must maintain attribution to the author(s) and the published article's title, journal citation, and DOI.

entropy barrier to replace the geometric constraint opens up the possibility of harnessing the shape of the constrained region to achieve control of the particle transport dynamics [26]. In recent years, particle diffusion through a confined structure has attracted a great deal of interest [7,27–29].

The focus of our paper is on particle diffusion dynamics through a confined structure that is periodic in space. A specific type of structure studied previously [30] is a channel formed via periodic contact with a series of uniformly spaced spherical cavities connected by a series of narrow openings, through which Brownian particles can cross the bottlenecks into other cells. The issues that have been studied include the diffusion coefficient [30] and the effective mobility [31] of Brownian particles. From the point of view of entropy [32], the phenomenon of the emergence of negative entropy values at certain parameter settings was uncovered [33] through calculating the change in the entropy potential of the whole periodic structure. This means that a negative migration rate associated with the particle movement would emerge, and this had been tested in an experiment of transport of yeast cells through this type of periodic structure, where the phenomenon of cell separation was observed [33]. A key assumption employed in previous theoretical studies of diffusion of Brownian particles through a periodic structure is that the particles have zero size, i.e., they are point particles.

In this paper, we investigate the interplay between particle size and Brownian transport through a restricted, periodic structure. The primary motivation of this problem is self-evident: In real-world applications, particles do have sizes. Intuitively, the size can have a significant effect on the transport dynamics. For example, in a simple term, it would be easier for small particles to go through but particles of sufficiently large sizes will be blocked. To be concrete, we study the paradigmatic structure of spherical cavities connected to each other through narrow channels and apply static and temporally periodic forcing in the direction of the channel. We consider hard-sphere particles and derive an effective channel boundary function, which is piece-wise smooth. Numerically, we carry out molecular dynamical simulations to study the diffusion dynamics in a systematic way. Theoretically, assuming that particle diffusion in the transverse cross section can reach an equilibrium rapidly, we invoke the concept of entropy barrier to treat the influence of the boundary constraint of the channel. This physical approach enables us to obtain analytic expressions for the key quantities underlying the diffusion dynamics such as the mean particle velocity and the effective diffusion coefficient, and their dependence on the particle size.

The main finding of this paper is the phenomenon of *current reversal*, which can be described, as follows. Our numerical calculations and theory reveal that, for particles of certain size, the direction of diffusion can be reversed when the forcing amplitude or the temporal asymmetric parameter of the forcing profile increases through a critical value that depends on the particle size. Thus, for a fixed forcing amplitude or a fixed value of the asymmetric parameter in an appropriate range, the mean diffusion velocity depends on the particle size. This is striking because it means that, for certain amplitude of the driving force, particles of different sizes can diffuse in opposite directions in the channel. In fact, there exists a critical value of the size: above which the particles

diffuse in one direction of the channel, but particles of sizes below the critical value diffuse in the opposite direction! Besides its fundamental importance in basic Brownian transport dynamics, this phenomenon provides a potential mechanism for separating particles of different sizes with applications in contexts such as transport through biological channels (e.g., separation of DNA fragments [34] and yeast cells) and separation of nanoparticles.

We use the term “current reversal” to refer to the situation where, under appropriate forcing, on average small and large particles can diffuse in opposite directions. That is, if the particle size is treated as a parameter, then as this parameter increases through a critical value, the direction of diffusion will be reversed. This should be distinguished from the previous studies [35,36] in which the particles were driven by a sinusoidal periodic force and an increase in the phase shift of the oscillating density at high frequencies can lead to a current reversal.

## II. MODEL DESCRIPTION AND PHYSICAL THEORY

### A. Brownian transport system with a periodic spherical structure

We consider a confined 2D periodic channel that is symmetric in the  $y$  direction, described by  $y = y_u(x) = -y_l(x)$ , as shown in Fig. 1. The geometric boundary functions of the periodic channel are defined by  $y_u(x)$  (the upper boundary) and  $y_l(x)$  (the lower boundary), which are given by

$$\begin{aligned} y_u(x) &= \sqrt{R^2 - (\bar{x} - l)^2} \\ y_l(x) &= -\sqrt{R^2 - (\bar{x} - l)^2}, \quad \bar{x} = \text{mod}(x, L), \end{aligned} \quad (1)$$

where  $L = 2l = 2\sqrt{R^2 - a^2}$  is the spatial period of the channel,  $\bar{x} = \text{mod}(x, L)$  is a modulo function to generate the periodic structure,  $a$  is the half-width of the bottleneck, and  $R$  is the radius of the semicircular structure of the upper (or lower) boundary of the channel within a single period. The maximum and minimum widths of the channel are  $2R$  and  $2a$ , respectively. With a hard spherical particle of radius  $r_p$  inside the periodic channel, the available space from the walls for particles depends on  $r_p$ . The upper effective half-width  $w_{e+}(x)$  is

$$w_{e+}(x) = \begin{cases} -\sqrt{r_p^2 - \bar{x}^2} + a, & 0 \leq \bar{x} < L_p, \\ \sqrt{(R - r_p)^2 - (\bar{x} - l)^2}, & L_p \leq \bar{x} < U_p, \\ -\sqrt{r_p^2 - (\bar{x} - L)^2} + a, & U_p \leq \bar{x} < L, \end{cases} \quad (2)$$

where  $L_p = r_p l / R$  and  $U_p = L - L_p$ . The lower effective boundary is described by  $w_{e-}(x) = -w_{e+}(x)$ . The effective channel width of a particle of radius  $r_p$  at any position in the periodic channel is

$$2w(x) = w_{e+}(x) - w_{e-}(x),$$

as shown by the dashed orange curves in Fig. 1, where the narrower reachable space for the centers of a hard-sphere particle of radius  $r_p$  is compared to that for a point particle.

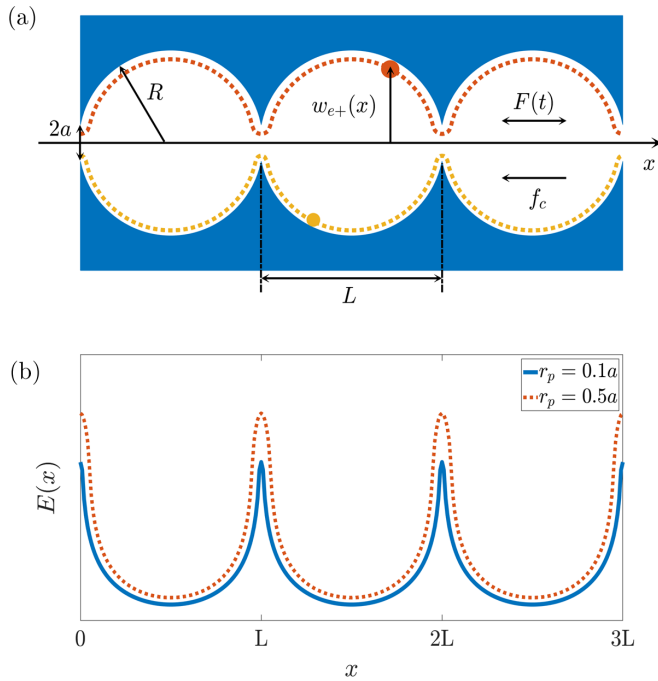


FIG. 1. Schematic diagram of a 2D periodic transport channel and entropic potentials. (a) Original periodic channel walls defined by the boundary function  $y_u(x)$  and  $y_l(x)$  [Eq. (1)], as indicated by the blue curves. The dashed orange curves represent the effective boundaries given by  $w_{e+}(x)$  and  $w_{e-}(x)$  [Eq. (2)], which confine the motion of spherical particles of radius ranging from  $r_p = 0$  to  $r_p = a$ . Particles with radii of  $r_p = 0.1a$  (yellow) and  $r_p = 0.5a$  (orange) are shown in the channel. The particles are driven by static and temporally periodic forcing. The value of the half-width parameter defined in Eqs. (1) and (2) is  $a = 0.1L$ . (b) The effective entropic potential for the two particle sizes depicted in (a), which is defined as  $E(x) = -\ln[2w_{e+}(x)]$ .

### B. Physical theory

The dynamics of a Brownian particle in a 2D periodic channel subject to a static force  $f_c$  and an oscillating force  $F(t)$  along the  $x$  direction can be described by the Langevin equation. In the over-damping regime, the equation reads

$$\gamma_r \frac{dx}{dt} = f_c + F(t) + \sqrt{\gamma_r k_B T} \xi_x(t), \quad (3)$$

$$\gamma_r \frac{dy}{dt} = \sqrt{\gamma_r k_B T} \xi_y(t), \quad (4)$$

where  $(x, y)$  specify the position of the particle center,  $k_B$  is the Boltzmann constant, and  $T$  is the absolute temperature. The frictional coefficient  $\gamma_r$  is given by the Stokes' law:  $\gamma_r = 6\pi\nu r_p$ , which depends on the viscosity  $\nu$  of the fluid and the radius  $r_p$  of the particle. The stochastic force  $\xi_{x,y}(t)$  is uncorrelated in time and modeled by white Gaussian noise with  $\langle \xi_i(t) \rangle = 0$  and  $\langle \xi_i(t) \xi_j(t') \rangle = 2\delta_{ij} \delta(t - t')$  ( $i, j = x, y$ ). In the over-damping regime, two basic assumptions hold for the diffusion system: (i) the particles are diluted (with small density) in the whole system and the fluid is viscous and (ii) each channel wall can be treated as a reflecting boundary. The two assumptions stipulate that, at low Reynolds numbers, all effects caused by particle-particle and wall-particle

interactions can be neglected, rendering diffusive the dominant dynamical behavior of the Brownian particles.

In a previous paper [27], an adjustable rectangular wave force  $F(t)$  was used, where particle separation was demonstrated. We adopt the following form of the periodic driving force:

$$F(t) = \begin{cases} \frac{1+\varepsilon}{1-\varepsilon} A, & n\tau \leq t < n\tau + \frac{1}{2}\tau(1-\varepsilon) \\ -A, & n\tau + \frac{1}{2}\tau(1-\varepsilon) < t \leq (n+1)\tau \end{cases}, \quad (5)$$

where  $\tau$  is the forcing period,  $A$  is its magnitude,  $n$  is an integer, and  $\varepsilon$  is a temporal asymmetric parameter with  $-1 \leq \varepsilon < 1$ . The temporal average of the force over one period  $\tau$  is zero. Different forms of the unbiased force can be realized through different choices of the value of  $\varepsilon$ . For  $\varepsilon = -1$ , we have  $F(t) = 0$ . For  $\varepsilon = 0$ ,  $F(t)$  reduces to a square wave form.

To make the Langevin equations dimensionless, we rescale the variables in Eqs. (3) and (4) by the characteristic spatial period  $L$  and the diffusion time:

$$t_D \equiv \gamma_{\max} L^2 / (k_B T),$$

where  $\gamma_{\max} = 6\pi\nu a$ . With these characteristic parameters, we introduce the dimensionless variables:  $\tilde{t} \equiv t/t_D$ ,  $\tilde{\tau} \equiv \tau/t_D$ ,  $\tilde{x} \equiv x/L$ ,  $\tilde{y} \equiv y/L$ ,  $\tilde{w}_{e+} \equiv w_{e+}/L$ , and  $\tilde{a} \equiv a/L$ . The rescaled forces are

$$\tilde{f}_c \equiv f_c L / k_B T,$$

$$\tilde{F}(\tilde{t}) \equiv F(t) L / k_B T.$$

To simulate particles in an external electrical field, we assume that the force depends linearly on the radius  $r_p$ . Specifically, we set  $f_1 = f_c a / r_p$  and  $f_0 = A a / r_p$ . (In the following, to simplify notation, we omit the hat in these quantities.)

The dimensionless form of the Langevin equations is

$$\frac{dx}{dt} = f_1 + F(t) + \sqrt{\frac{a}{r_p}} \xi_x(t), \quad (6)$$

$$\frac{dy}{dt} = \sqrt{\frac{a}{r_p}} \xi_y(t), \quad (7)$$

where the dimensionless force is given by

$$F(t) = \begin{cases} \frac{1+\varepsilon}{1-\varepsilon} f_0, & n\tau \leq t < n\tau + \frac{1}{2}\tau(1-\varepsilon) \\ -f_0, & n\tau + \frac{1}{2}\tau(1-\varepsilon) < t \leq (n+1)\tau \end{cases}. \quad (8)$$

The dynamics of a confined over-damped Brownian particle, as governed by Eqs. (6) and (7), can be analyzed through the concept of entropic potential and the corresponding Fick-Jacobs equation[18,20,21,37]:

$$\frac{\partial P(x, t)}{\partial t} = \frac{\partial}{\partial x} \left\{ D(x) \left[ \frac{\partial P}{\partial x} + V'(x) P \right] \right\} = -\frac{\partial j}{\partial x}, \quad (9)$$

where  $P(x, t)$  is the joint probability density function and  $j(x, t)$  is the probability flux. The free energy  $V(x)$  is defined as

$$V(x) = U - TS(x) = -[f_1 + F(t)] \left( \frac{r_p}{a} \right) x - \ln[2w_{e+}(x)], \quad (10)$$

where

$$TS(x) = \ln[2w_{e+}(x)], \quad \text{and}$$

$$U = -[f_1 + F(t)](r_p/a)x$$

denote the entropic and energy contributions, respectively. The Fick-Jacobs equation (9) can be obtained from the 2D Smoluchowski equation after eliminating the  $y$  coordinate. The reduction entails an effective position-dependent diffusion coefficient defined as

$$D(x) = \frac{a}{r_p[1 + w'_{e+}(x)^2]^{1/3}}. \quad (11)$$

The particle current is a key quantity characterizing the transport dynamics through a periodic channel structure, which can be derived from the Fick-Jacobs approximation. From Eq. (9), we have

$$j(x, t) = -D(x) \left[ \frac{\partial P}{\partial x} + V'(x)P \right], \quad (12)$$

where  $P(x, t)$  satisfies the normalization condition  $\int_0^1 P(x, t) dx = 1$  and the condition of periodicity  $P(x, t) = P(x + 1, t)$ . After a lengthy algebraic manipulation (Appendix A), we obtain in the adiabatic limit the mean velocity as

$$\langle v \rangle = \frac{1}{\tau} \int_0^\tau J[F(t)] dt = \frac{1}{2}(J_1 + J_2), \quad (13)$$

where

$$J_1 = (1 - \varepsilon)J\left(\frac{1 + \varepsilon}{1 - \varepsilon}f_0\right) \text{ and } J_2 = (1 + \varepsilon)J(-f_0), \quad (14)$$

and the current  $j(f_0)$  is given by the Stratonovich formula [38–40] as

$$J(f_0) = \frac{1 - e^{-(f_1+f_0)r_p/a}}{\int_0^1 dx \frac{e^{V(x)}}{D(x)} \int_{x-1}^x dy e^{-V(y)}}. \quad (15)$$

It should be noted that our theoretical approach based on analyzing the Fick-Jacobs equation is standard in the literature. For example, a similar analysis but for a different 2D channel was carried out by Ai [41].

### III. SIMULATION OF BROWNIAN DYNAMICS

We carry out direct numerical simulations of Brownian dynamics based on the dimensionless Eqs. (6), (7), and Eq. (13), and to compare the theoretical and numerical results. In particular, we use the stochastic Euler algorithm to simulate Eqs. (6) and (7), where single-step integration is proceeded as

$$x(t+h) = x(t) + [f_1 + F(t)]h + \sqrt{\frac{2ah}{r_p}}\xi_1, \quad (16)$$

$$y(t+h) = y(t) + \sqrt{\frac{2ah}{r_p}}\xi_2, \quad (17)$$

with  $\xi_1$  and  $\xi_2$  being two Gaussian random numbers of unit variance. Particle positions falling outside of the channel can be dealt with using the reflected boundary conditions at the channel walls, i.e., the channel boundaries constrain the particles in the system via fully elastic collisions. To improve the accuracy and minimize the statistical errors, we use over  $10^3$  random realizations and choose the time step  $h = 10^{-4}$ . An initial particle distribution at  $t = 0$  starts from the center of a cell. The new positions for each realization along the  $x$  and

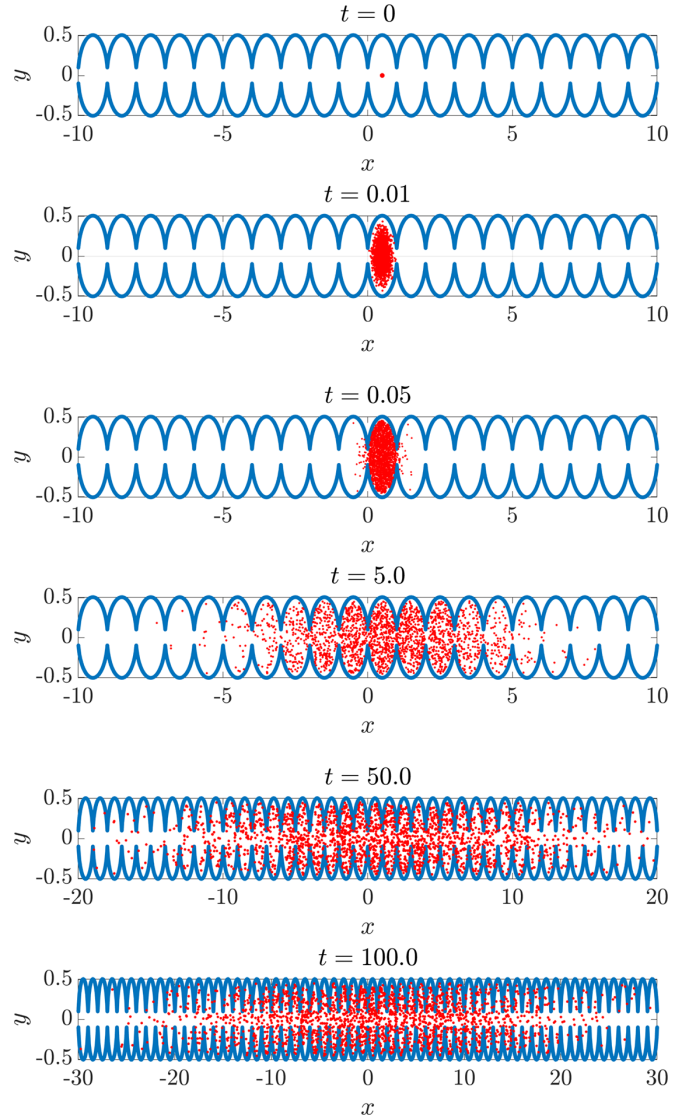


FIG. 2. Numerically obtained snapshots of the distribution of Brownian particles at different times in the absence of external forcing. The structure is a symmetric 2D channel with the geometric boundary defined by Eq. (2). The six snapshot images are obtained at  $t = 0, 0.01, 0.05, 0.1, 1.0$ , and  $10$ . The initial distribution of the Brownian particles start at the middle of a cell, at time  $t = 0$  (top panel). After diffusion within the channel geometry and in the long time limit, the distribution reaches a steady state (bottom panel). The value of the temporal asymmetric parameter is  $\varepsilon = -1$ . The static force is set to  $f_1 = 0$ . The number of particles is 1000. Other parameter values are  $L = 1$ ,  $a = 0.1L$ , and  $r_p = 0.1a$ .

$y$  directions are determined by Eqs. (16) and (17). The mean particle velocity along the  $x$  direction is defined as

$$\langle v \rangle = \langle \dot{x} \rangle = \lim_{t \rightarrow \infty} \frac{\langle x(t) - x(0) \rangle}{t}. \quad (18)$$

Figure 2 presents a series of numerically calculated snapshots of the particle distribution at six different time instants to illustrate the diffusion process of the Brownian particles in a symmetric 2D channel in the absence of any external force. In this case, the particle diffusion dynamics are solely determined by the random (thermal) fluctuations in the

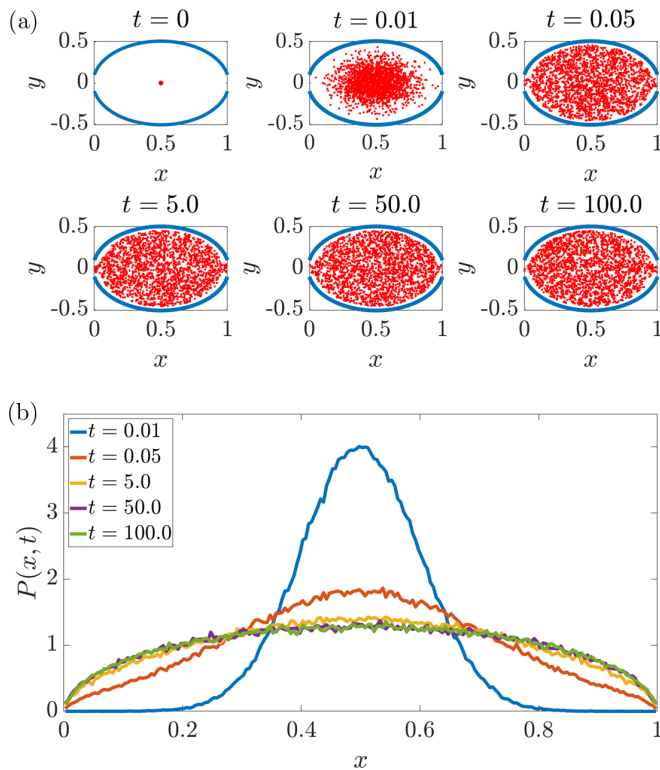


FIG. 3. Nondirectional diffusion in the absence of external forcing. (a) Distribution of Brownian particles (1000) mapped into a single unit cell of the 2D channel defined by Eq. (2) with  $L = 1$ ,  $a = 0.1L$ , and  $r_p = 0.5a$  for six different instants of time, where the original distributions at those time instants are shown in Fig. 2. The number of particles is 1000. (b) Probability distribution  $P(x, t)$  of the Brownian particles in the  $x$  direction within a single cell at different time instants. Note that the distributions for  $t = 50.0$  and  $t = 100.0$  are nearly identical, indicating that a steady state has been reached.

environment. At  $t = 0$ , the ensemble of Brownian particles is located about the center of a single cell. Thermal noise makes the particles diffuse randomly and the particles redistribute over the available space within the channel geometry before reaching a steady state. It is worth noting that, since the channel is periodic and thus infinitely long, the particles always continue to spread along the channel, i.e., there is no equilibrium state for the whole system. However, all the diffusive particles can be mapped into a single unit cell and their distribution can become stable. The term “steady state” is used to indicate that the particles have reached such a stable distribution. Because of the absence of external driving, the respective probabilities for the particles to spread to the left and right are the same. As shown in Fig. 2, the Brownian particles diffuse evenly from their initial positions to both sides and the associated transport behavior is not directional. During the diffusion process, the particles may cross a large number of cells.

To better illustrate the behavior of particle diffusion and to ascertain the emergence of a steady-state distribution, we map the particles in the spatially periodic system into a single unit cell. The distributions of the particles at the six time instants are shown in Fig. 3(a). Figure 3(b) shows the corresponding normalized probability distribution in the  $x$  direction (the

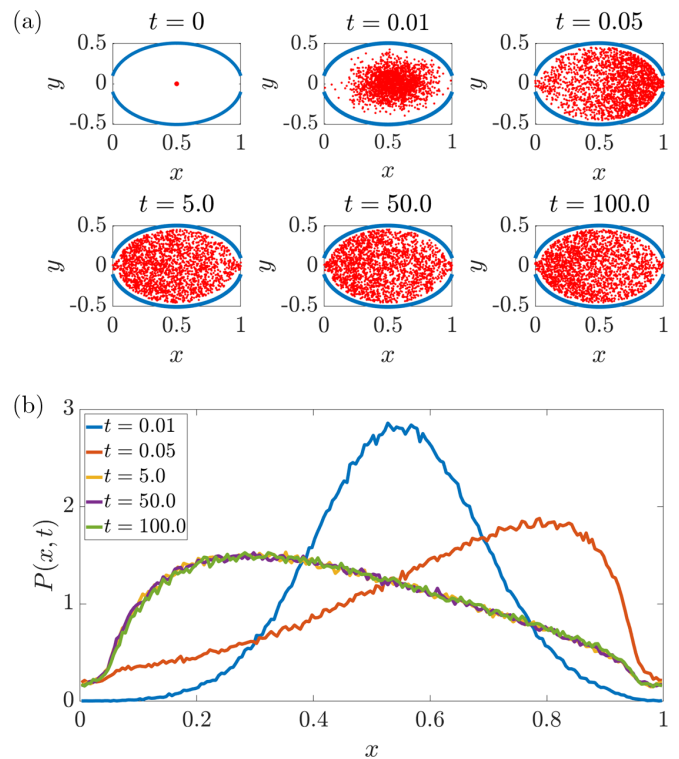


FIG. 4. Directional transport induced by periodic forcing. (a) Numerically obtained density snapshots of the Brownian particles (1000) at different instants of time in a symmetric 2D channel with the structure defined by Eq. (2), which are mapped into a single unit cell. The periodic forcing amplitude is  $f_0 = 1$  and the asymmetry parameter value is  $\varepsilon = 0.7$ . In addition, Brownian particles are driven by a constant force  $f_1 = -1$ . The upper row corresponds to  $t = 0, 0.01$ , and  $0.05$  (left to right), and the bottom row corresponds to  $t = 5.0, 50.0$ , and  $100.0$  (left to right). The number of particles is 1000. (b) Probability distribution  $P(x, t)$  within a unit cell in the  $x$  direction at different time instants.

direction of channel). At  $t = 0$ , the initial particle distribution is a delta function. The distribution then broadens as time progresses. The peak of the probability density at the center of the distribution decreases gradually, and the probability density values on both sides gradually increase. The distribution finally reaches a steady state. For any  $t > 0$ , the probability distribution shown in Fig. 3(b) is symmetric with respect to the initial position at different time, indicating lack of any directional transport.

To assess the effect of an external force on particle diffusion, we set the periodic forcing amplitude to be  $f_0 = 1.0$  and choose the value of the temporal asymmetric parameter to be  $\varepsilon = 0.7$ . Moreover, we apply a static force in the negative direction:  $f_1 = -1$ . Figure 4(a) shows the numerically calculated density snapshots of the particles at different time  $t$  mapped into a single unit cell. Initially at  $t = 0$ , all particles are located about the center of a unit cell. After a short period of time (e.g.,  $t = 0.01$  and  $t = 0.05$ ), the positive part of the periodic force governs the diffusion process, so most particles migrate to the right half of the channel. The negative phase of the periodic force and the negative static force then kick in, affecting the diffusion of particles. For example, at  $t = 5.0$ ,

$t = 50.0$ , and  $t = 100.0$ , the particle distributions have a component in the left half of the channel, as shown in Fig. 4(b), the normalized probability distribution. For  $t \geq 100.0$ , the diffusion dynamics have reached a steady state, with the corresponding normalized probability distribution shown in Fig. 4(b), which is *asymmetric* with most particles on the left side of the channel. We thus see that a periodic force can lead to directional transport of Brownian particles.

#### IV. MAIN RESULTS: CURRENT REVERSAL AND PARTICLE SEPARATION

Figure 4 demonstrates that Brownian particles subject to entropic barriers and driven by static and periodic forcing are capable of directional transport when diffusing through a symmetric confined structure. Here we focus on a key quantity characterizing the transport: the mean particle velocity  $\langle v \rangle$ , and compare the analytic prediction [Eq. (13) in Sec. II B] with the numerical results from simulations of Eq. (18). To be concrete, in the following we fix all geometric parameters of the periodic transport channel and set its spatial period to be  $L = 1$ . In addition, we set the half width of the bottleneck to be  $a = 0.1L$ .

##### A. Current reversal and particle separation

Figure 5(a) shows the numerical results of the mean velocity  $\langle v \rangle$  as a function of the periodic forcing amplitude  $f_0$  for five different values of  $r_p$ , the particle radius. For relatively small values of the amplitude ( $0 \leq f_0 < 2.25$ ), the negative force exerted on the particles plays a dominant role in transport, causing all particles to move toward the left. As the amplitude increases, a mean current of the particles with different sizes begins to rise, because the positive component of the periodic driving force begins to offset the negative static force. For example, for  $f_0 = 15.0$ , the positive phase of the periodic force dominates particle transport in the channel, resulting in a net positive mean velocity. In this case, the average velocity is positive for particles of all five different sizes. As can be seen from the entire velocity curves in Fig. 5(a), the absolute value of the average velocity  $|\langle v \rangle|$  decreases to zero and then increases. During this process, current reversal can be observed. For particles of radius  $r_p = 0.1a$ , the amplitude of the periodic force is 15.0 when current reversal occurs. For particles of radius  $r_p = 0.9a$ , current reversal occurs with  $f_0 = 2.25$ . For particles of radius  $r_p = 0.3a, 0.5a, 0.7a$ , the critical amplitude of current reversal occurs between 2.25 and 15.0. For  $2.25 < f_0 \leq 15.0$ , the mean velocity  $\langle v \rangle$  is negative for small values of  $r_p$  but positive for large values of  $r_p$ , i.e., small particles move towards left and large particles move towards right, realizing particle separation.

Figure 5(b) shows the mean velocity as a function of  $r_p$  for three different values of the forcing amplitude:  $f_0 = 0, 2.0$ , and 15.0. For  $f_0 = 0$  and  $f_0 = 2.0$ , The current is negative for all particles with radii between  $r_p = 0.1a$  and  $r_p = 0.9a$ . In this case, all particles move toward the left of the channel, and small particles have a large negative mean velocity. For  $f_0 = 15.0$ , the current is positive for all values of  $r_p$  and exhibits a monotonic behavior: the larger the radius of the particles, the faster the mean motion. Figure 5(c) presents three

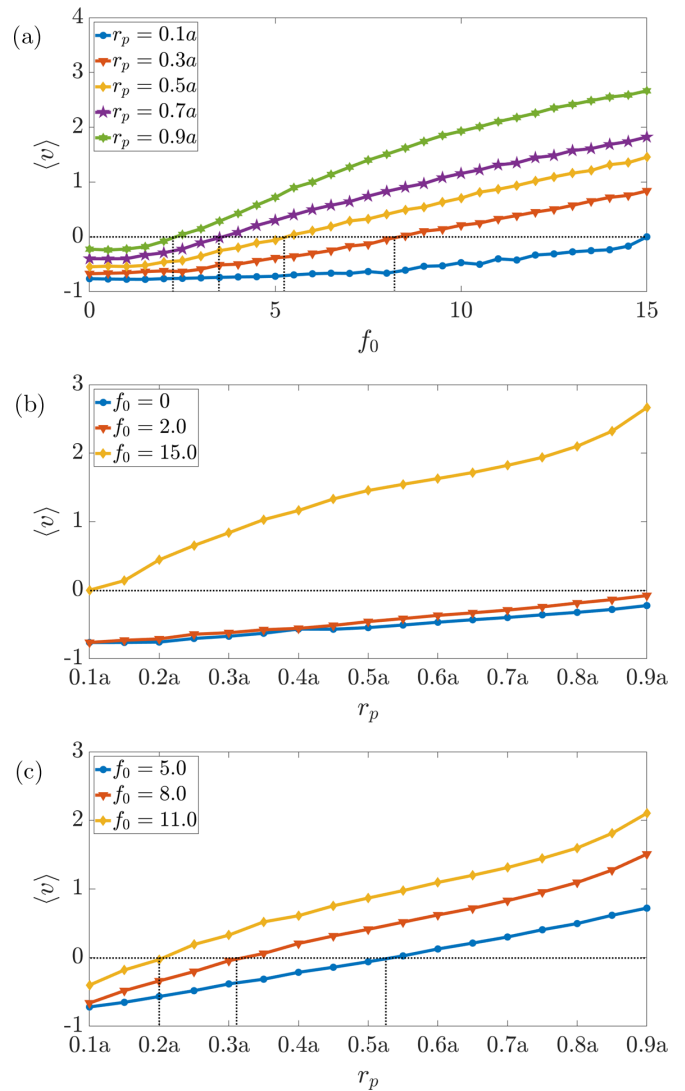


FIG. 5. Demonstration of current reversal and particle separation. (a) Mean particle velocity  $\langle v \rangle$  vs the periodic forcing amplitude  $f_0$  for five values of the particle size. (b) Regime of relatively small and large forcing amplitude, in which the particles diffuse in the same direction. Shown is the mean current vs the particle radius for  $f_0 = 0, 2.0$ , and 15.0. (c) Explicit demonstration of the phenomenon of particle separation:  $\langle v \rangle$  vs  $r_p$  for  $f_0 = 5.0, 8.0$ , and  $f_0 = 11.0$ . In each case, a critical radius emerges: particles of size smaller than it have a negative mean velocity while those larger than it have a positive mean velocity. The critical radius value depends on the forcing amplitude. In all cases, the value of the temporal asymmetric parameter is set to be  $\varepsilon = 0.7$  and the static force is  $f_1 = -1$ .

cases explicitly demonstrating the separation phenomenon for  $f_0 = 5.0, 8.0$ , and  $f_0 = 11.0$ , where the direction of  $\langle v \rangle$  depends on the particle radius and particles of different sizes move in different directions on average. There is a threshold radius  $r_p^c$ : particles smaller than  $r_p^c$  move to the left, whereas particles larger than that move to the right. When the amplitude is set to  $f_0 = 5.0$ , the threshold radius  $r_p^c$  equals  $0.525a$ . For  $f_0 = 8.0$  and  $f_0 = 11.0$ , the threshold radii are  $r_p^c = 0.31a$  and  $r_p^c = 0.2a$ , respectively. In the regime of particle separation, the critical radius depends on the forcing amplitude  $f_0$ .

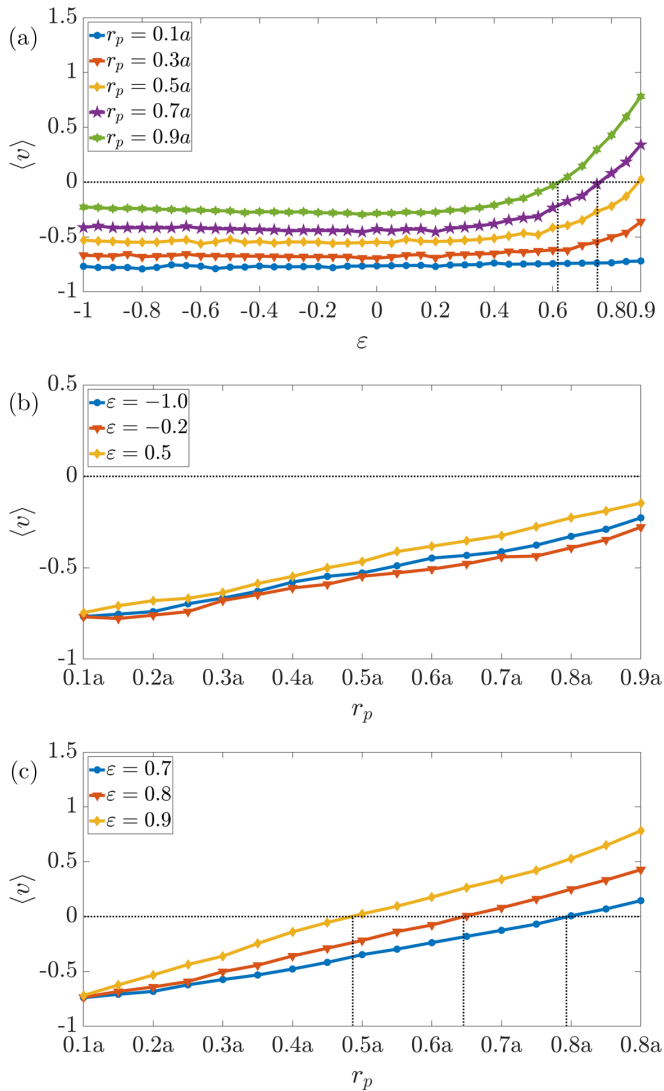


FIG. 6. Current reversal and particle separation induced by asymmetry in the external forcing. (a) Mean particle velocity  $\langle v \rangle$  vs the temporal asymmetric parameter  $\varepsilon$  for five values of the particle size. (b) Regime of relatively small value of  $\varepsilon$ , in which particles diffuse in the negative direction. Shown is the mean current  $\langle v \rangle$  vs the particle radius for  $\varepsilon = -1.0, -0.2$ , and  $0.5$ . (c) Evidence for particle separation:  $\langle v \rangle$  vs  $r_p$  for  $\varepsilon = 0.7, \varepsilon = 0.8$ , and  $\varepsilon = 0.9$ . In both panels, the value of the forcing amplitude is  $f_0 = 3$  and the static force is  $f_1 = -1$ .

The direction and magnitude of particle diffusion not only can be controlled by varying the amplitude of the external force but can also be modulated by adjusting the temporal asymmetric parameter  $\varepsilon$ . Figure 6(a) shows  $\langle v \rangle$  vs  $\varepsilon$  for  $f_0 = 3$  and  $f_1 = -1$ . Tuning the value  $\varepsilon$  enables control of the transport velocity and direction. In particular,  $\langle v \rangle$  is negative for  $-1 \leq \varepsilon < 0.62$  because, in this case, the unbiased external periodic force is asymmetric and the positive phase of the periodic driving force does not cancel out the negative phase and the negative static force  $f_1$ . For  $0.62 < \varepsilon \leq 0.9$ , the mean velocity  $\langle v \rangle$  goes from negative to positive, i.e., the current reverses its direction for some critical value of  $\varepsilon$ , where the critical value depends on the size of the particle. For

particles with  $r_p = 0.1a$  and  $r_p = 0.3a$ , their mean velocity  $\langle v \rangle$  is always negative over the whole range of  $\varepsilon$  values considered. For particles with  $r_p = 0.5a, 0.7a$ , and  $0.9a$ , the critical values are  $\varepsilon_c \approx 0.90, \varepsilon_c \approx 0.75$ , and  $\varepsilon_c \approx 0.62$ , respectively. This indicates that the larger the particle size, the smaller the threshold parameter  $\varepsilon$  is required for current reversal. Figure 6(a) also demonstrates that particles of different sizes will have different diffusion directions when the temporal asymmetric parameter  $\varepsilon$  is between  $0.62$  and  $0.9$ , suggesting that a better separation efficiency can be achieved for Brownian particles.

As Fig. 6(a) implicates, changing the value of the temporal asymmetric parameter  $\varepsilon$  can induce Brownian particles to diffuse in opposite directions. This is explicitly demonstrated in Figs. 6(b) and 6(c), which show  $\langle v \rangle$  vs  $r_p$  for different values of  $\varepsilon$ . Note that the radius of the particle is set between  $0.1a$  and  $0.9a$ . As shown in Fig. 6(b), for  $\varepsilon = -1, \varepsilon = -0.2$ , and  $\varepsilon = 0.5$ , we have  $\langle v \rangle < 0$ , regardless of the particle size. For these three sets of parameters, particles move in the same direction. However, for  $\varepsilon = 0.7, \varepsilon = 0.8$ , and  $\varepsilon = 0.9$ , the Brownian particles larger than a given critical radius diffuse to the right, whereas particles smaller than that diffuse to the left. As depicted in Fig. 6(c), the value of the threshold radius depends on  $\varepsilon$ . For  $\varepsilon = 0.7, 0.8$ , and  $0.9$ , the critical radii  $r_p^c$  are  $0.79a, 0.65a$ , and  $0.48a$ , respectively. This indicates that the efficiency of distinguishing and separating particles can be improved by properly choosing the value of  $\varepsilon$ .

Figure 7 presents a comparison between the analytic results from the Fick-Jacobs equation (solid curves) and numerical results from Brownian dynamical simulation (symbols). In Fig. 7(a), the mean velocity vs  $f_0$  for  $0 \leq f_0 \leq 5.0$  for two particle sizes is shown. For  $r_p = 0.7a$ , the agreement between theory (blue solid curve) and the simulation results is good for  $0 \leq f_0 < 3.0$ . For  $r_p = 0.9a$ , the agreement is reasonable for  $0 \leq f_0 < 2.5$ . For larger values of  $f_0$ , the theoretical prediction deviates from the numerical results. (See Sec. V for a detailed analysis of the validity of the theory.) Figure 7(b) shows  $\langle v \rangle$  vs  $\varepsilon$  for  $r_p = 0.7a$  and  $r_p = 0.9a$ . Since current reversal occurs only for positive values of  $\varepsilon > 0$ , we set its range of variation to be  $[0, 0.9]$ . For  $r_p = 0.7a$  (the blue curve and symbols), the agreement between theory and numerical results is reasonable for  $0 \leq \varepsilon < 0.75$ . For  $r_p = 0.9a$ , the range of agreement is  $0 \leq \varepsilon < 0.65$ . Note that, in both cases, current reversal occurs in the range of agreement.

## B. A systematic analysis of current reversal

We carry out a systematic analysis of the phenomenon of current reversal as demonstrated in Figs. 5 and 6. Especially, Fig. 5(a) shows that the mean velocity changes from negative to positive as the forcing amplitude  $f_0$  increases, and particles of different sizes require a different value of  $f_0$  to make the transition. Analogously, in Fig. 6(a), as the temporal asymmetric parameter  $\varepsilon$  increases from  $-1$  to  $0.9$ , current reversal occurs. These results indicate that both parameters can be exploited to induce a change in the direction of diffusion of Brownian particles. Another essential parameter is the particle radius  $r_p$ . To obtain a more comprehensive picture of current reversal, we investigate the behavior of the mean velocity with respect to systematic variations in the three parameters.

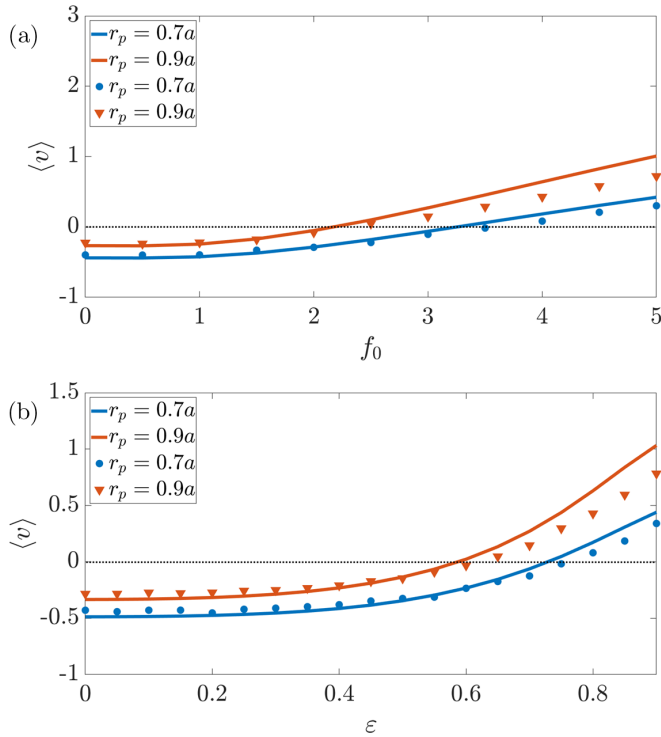


FIG. 7. Comparison between numerical and theoretical results. (a) Mean velocity  $\langle v \rangle$  vs  $f_0$  for  $\epsilon = 0.7$ . (b) Mean velocity  $\langle v \rangle$  vs  $\epsilon$  for  $f_0 = 3$ . In both panels, the solid lines represent the theoretical predictions and the symbols are numerical results. Two particle sizes are used:  $r_p = 0.7a$  and  $r_p = 0.9a$ . Other parameter values are  $f_1 = -1$ ,  $L = 1.0$ , and  $a = 0.1L$ .

Figure 8(a) shows the numerical contour plot of the mean velocity  $\langle v \rangle$  in the  $(r_p, f_0)$  parameter plane. For clarity, we divide Fig. 8(a) into two areas. In Area 1,  $\langle v \rangle$  is negative for  $0 < f_0 < 2.25$ , i.e., all particles move to the left of the channel, indicating that relatively weak forcing amplitude leads to a negative mean current. This can be understood by noting that, while the unbiased external force is temporally periodic, its negative component plays a key role in the transport process aided by the static force  $f_1$ . As a result, a net negative current is produced. In Area 2, current reversal is possible. In particular, the orange solid curve corresponds to zero current, across which current reversal occurs. For  $2.25 < f_0 < 15.0$ , the current is negative for small values of  $r_p$  but becomes positive for large values of  $r_p$ . The critical radius  $r_p^c$  for particle separation depends on the value of  $f_0$ , as represented by the orange solid curve, which gives the threshold radius  $r_p^c$  for any given  $f_0$  in the range.

Similarly, Fig. 8(b) shows the contour of  $\langle v \rangle$  in the  $(\epsilon, r_p)$  plane, where the orange solid curve is the zero-current contour. As shown in Fig. 6(a), when current reversal occurs, the range of the temporal asymmetric parameter is  $0.62 < \epsilon \leq 0.9$ . In order to show the details of current reversal, we set the range of the  $\epsilon$  values to be  $[0, 0.9]$  in Fig. 8(b). There are two distinct areas. In Area 1 ( $0 \leq \epsilon < 0.62$ ),  $\langle v \rangle$  is negative for all particles. In Area 2 ( $0.62 < \epsilon \leq 0.9$ ), current inversion can be observed. Analogously, the orange solid curve corresponds to  $\langle v \rangle = 0$ , across which current reversal occurs. It is worth noting that particles with radius less than  $0.48a$  do

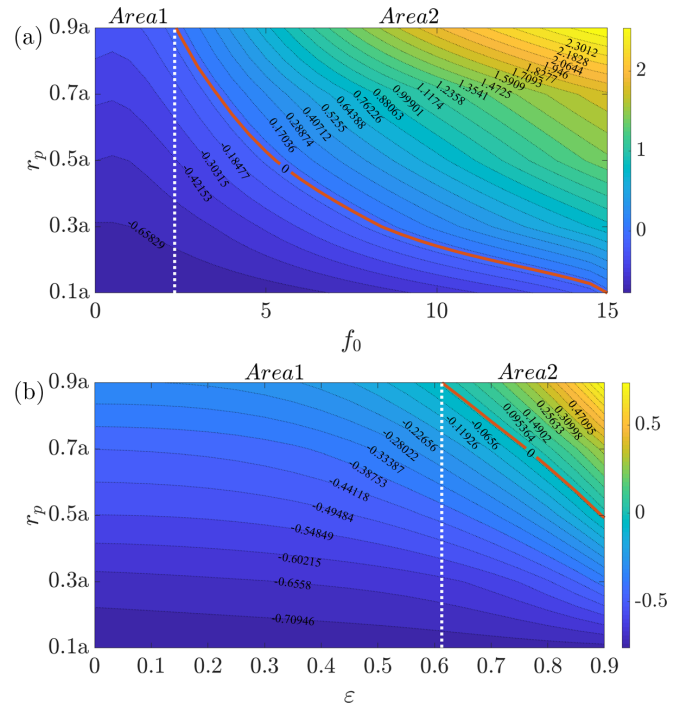


FIG. 8. Contour plot of mean velocity  $\langle v \rangle$ . (a) Contour plot in the parameter plane  $(f_0, r_p)$  for  $\epsilon = 0.7$ . The black dotted curves denote the contours of  $\langle v \rangle \neq 0$ . The orange solid curve is the zero-current contour, across which current reversal occurs. (b) Contour plot in the parameter plane  $(\epsilon, r_p)$  for  $f_0 = 3$ . The orange solid curve represents zero-current contour in the diagram. In both panels, the static force is set to  $f_1 = -1$ . The parameter values of the channel structure are  $L = 1.0$  and  $a = 0.1L$ .

not experience current reversal. For  $0.62 < \epsilon \leq 0.9$ , particles smaller than a given threshold radius  $r_p^c$  move to the left of the channel, whereas particles larger than that move towards the right. The threshold radius  $r_p^c$  for particle separation depends on the value of  $\epsilon$ , as indicated by the orange solid curve (zero currents) in Fig. 8(b).

### V. APPLICABILITY OF THEORY

In the regime of weak forcing and weak asymmetry, our numerical results in Sec. IV agree with the theoretical prediction reasonably well. As our theory is approximate, it is necessary to study the range of its applicability. The starting point of our validity analysis is the derivation of the Fick-Jacobs equation Eq. (9), in which equilibrium dynamics in the direction transverse to particle transport are assumed. The resulting theoretical predictions are thus expected to be accurate when this hypothesis holds. Previously, to obtain the conditions under which the equilibrium hypothesis is reasonable, a method based on analyzing the different time scales involved in confined transport was proposed [24]. In particular, for particle diffusion in a two-dimensional periodic channel, different characteristic processes in the axial direction can be identified, which correspond to different time scales that can be derived from the Langevin equations [(3) and (4)]. For diffusion in the  $y$  direction over a distance  $\Delta y$ , in the absence

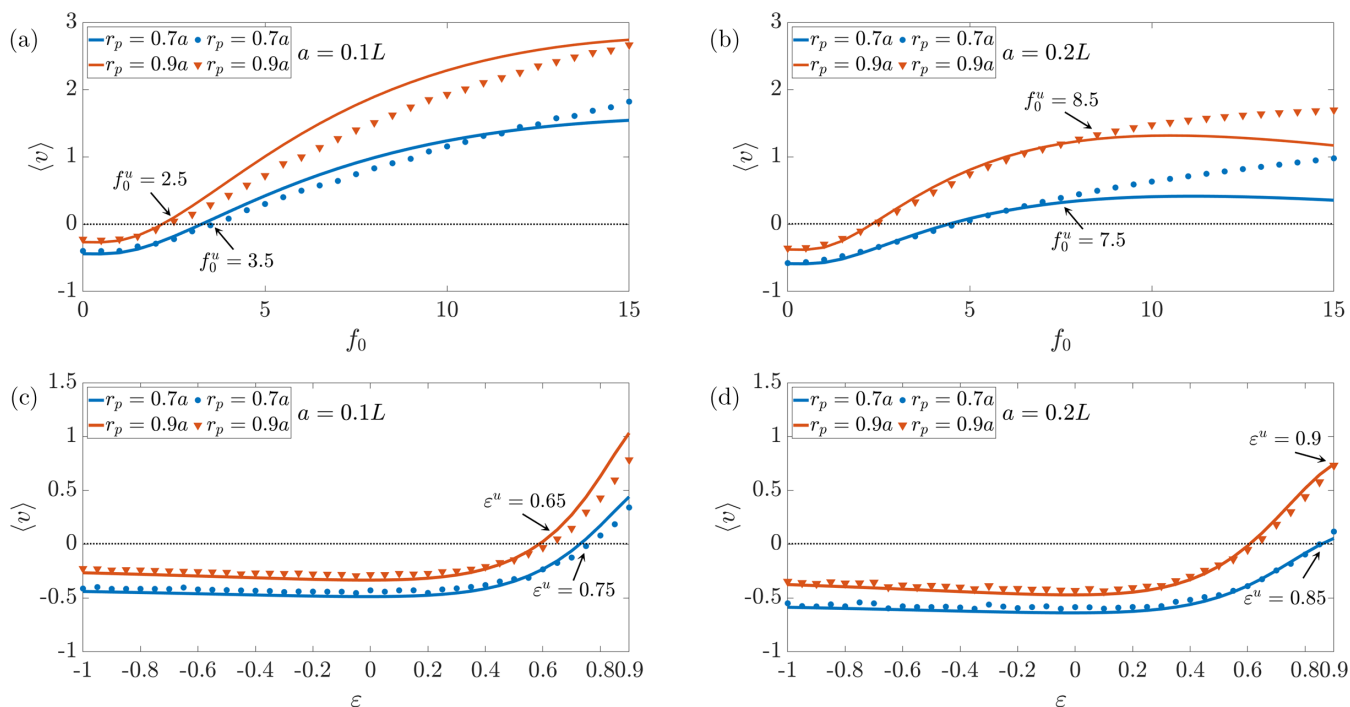


FIG. 9. Comparison between the numerical and theoretical results. [(a), (b)] Mean velocity  $\langle v \rangle$  vs  $f_0$  for  $a = 0.1L$  and  $a = 0.2L$ , respectively, for  $\varepsilon = 0.7$ . Two particle sizes are used:  $r_p = 0.7a$  and  $r_p = 0.9a$ . For both sizes, there is a reasonable agreement between the theoretical predictions (solid curves) and numerical results (symbols) in the weak forcing regime. For the smaller particle size, the agreement holds approximately for the entire range of the forcing amplitude illustrated. For the larger particle size in (b), the agreement begins to deteriorate as the forcing amplitude increases through about 8.0, due to the breakdown of the transverse equilibrium condition. [(c),(d)] Mean velocity  $\langle v \rangle$  vs  $\varepsilon$  for  $a = 0.1L$  and  $a = 0.2L$ , respectively, for  $f_0 = 3.0$ . Since the forcing amplitude is relatively small, in all cases there is a good agreement between the theory and numerical results. Other parameter values are  $f_1 = -1$  and  $L = 1.0$ .

of any external force, the characteristic time is given by

$$\tau_y = \frac{\Delta y^2}{2D}, \quad (19)$$

where  $D = k_B T / \gamma_r$ . Similarly, the characteristic time associated with diffusion in the  $x$  direction is

$$\tau_x = \frac{\Delta x^2}{2D}. \quad (20)$$

In order to achieve an equilibrium in the transverse direction, we must have  $\tau_y \ll \tau_x$ , which requires

$$\frac{\Delta y^2}{\Delta x^2} \sim w_{e+}^2(x) \ll 1. \quad (21)$$

The inequality (21) is a local condition under which the Fick-Jacobs equation holds. To obtain a global condition for the whole transport channel, we average the local criterion over one spatial period  $L$  of the channel:

$$\langle w_{e+}^2(x) \rangle = \int_0^L w_{e+}^2(x) dx. \quad (22)$$

A focal point of our work is to study the limiting effects of the channel on particle transport to understand the complex dynamical process in restricted channels in the real world, which is the reason that we set the half width of bottleneck to  $a = 0.1L$ . In this case, the value of  $\langle w_{e+}^2(x) \rangle$  is about 1.36, which violates the condition (21) and lead to a disagreement

between the theoretical and numerical results. Increasing the half width will reduce the value of  $\langle w_{e+}^2(x) \rangle$ . For example, for  $a = 0.15L$ , we have  $\langle w_{e+}^2(x) \rangle \approx 1.0$ . For  $a = 0.2L$ , we have  $\langle w_{e+}^2(x) \rangle \approx 0.77 < 1$ , in which case a better agreement between the theory and numerical results can be anticipated. Note that, increasing the value of  $a$  above, e.g.,  $0.3L$ , would effectively flatten the channel boundary and make the transport dynamics trivial.

To verify that a larger value of the bottleneck width than  $0.1L$  can result in an improved agreement between the theory and numerical results, we calculate the the mean velocity  $\langle v \rangle$  as a function of  $f_0$  and  $\varepsilon$ , for the two cases of  $a = 0.1L$  and  $a = 0.2L$  (for comparison). The results are shown in Fig. 9, for two representative particle sizes. Specifically, Fig. 9(a) indicates that, for  $a = 0.1L$ , the theoretical predictions deviate from the numerical results as  $f_0$  exceeds the threshold value  $f_0^u \approx 3.0$ , but for  $a = 0.2L$ , the agreement holds until about  $f_0^u \gtrsim 8.0$ , as shown in Fig. 9(b). Similar improvement in the agreement between the theory and numerical results is observed when the temporal asymmetric parameter  $\varepsilon$  systematically increases, as shown in Figs. 9(c) and 9(d) where, for  $a = 0.1L$ , the theoretical prediction holds until for  $\varepsilon = \varepsilon^u \approx 0.7$ , but for  $a = 0.2L$ , this threshold value becomes  $\varepsilon^u \approx 0.9$ .

The above analysis of the deviations between numerical and theoretical results focuses on the conditions under which equilibrium dynamics in the direction transverse to particle transport can be achieved. For example, if the forcing

amplitude is too large, the Brownian particles will be strongly pulled in the  $x$  direction during some time periods so that the particles are not able to reach the diffusion equilibrium in the  $y$  direction fast enough for the equilibrium assumptions to hold. Another factor that can contribute to the deviations is  $D(x)$ , the effective position-dependent diffusion coefficient that is a basic quantity in the Fick-Jacobs equation. It is given by the Reguera-Rubi formula in Eq. (11) that contains the spatial derivative of the channel boundary. While the validity of this formula has been checked in certain cases (e.g., for the channel formed by overlapping circles [42]), near the cusps where the derivative diverges, the formula is not applicable. We also observe from Fig. 9 that the deviations tend to increase with the forcing amplitude, which can be due to the effects of forcing on the diffusion coefficient. Indeed, it was shown rigorously [43] that, for a strictly one-dimensional system,  $D(x)$  depends on the driving force.

## VI. DISCUSSION

We have studied the diffusion dynamics of finite size Brownian particles through in a confined channel with a spatially periodic spheroidal structure. Theoretically, the 2D diffusive dynamics can be analyzed using the method of dimension reduction, leading to the paradigmatic 1D stochastic Fick-Jacobs equation. Direct Brownian molecular dynamics simulations of the full system in terms of a key quantity characterizing the transport dynamics, the mean particle velocity, provide strong support for the applicability of the Fick-Jacobs equation to the diffusion system. The roles of the parameters defining the external periodic forcing, such as its amplitude and the temporal asymmetric parameter, as well as the particle radius, in the transport dynamics have been studied in detail, opening a door to controlling the diffusive dynamics of finite-sized Brownian particles through a confined structure [26].

Our paper has unveiled two mechanisms to modulate the transport behavior. In particular, distinct directional motions as characterized by the mean directional current can be induced by (a) varying the forcing amplitude and (b) tuning the temporal asymmetric parameter. When only a static force is applied in the negative direction, all particles move towards the left. When both static and periodic forcing are present, a net positive current can emerge in the channel. For a fixed periodic forcing amplitude, the current depends strongly on the particle size, enabling separation of particles of different sizes through the differential particle velocity. Likewise, varying the temporal asymmetric parameter can enhance or suppress the directional transport. When this parameter value is small, all particles follow the negative static force and move towards the left of the channel. As the value of the parameter increases, the mean velocity of the particles in the negative direction gradually decreases to zero and then increases in the positive direction, leading to the phenomenon of current reversal. The critical value of the temporal asymmetric parameter for current reversal depends on the particle size.

Our work has revealed that, under appropriate conditions, the diffusive motions of particles of different sizes can occur in opposite directions. Especially, a threshold in the particle size emerges, where particles of size larger than or smaller than the threshold value move in opposite directions. This

provides a mechanism for separating particles of different sizes. Intuitively, varying the profile of the external force can modulate the particle motion in general, but our work brings forth a detailed and quantitative understanding of how the diffusion dynamics of Brownian particles may be controlled, and this will have applications in a variety of transport systems that arise ubiquitously in physical and biological sciences.

The finding of the present paper is based on single-particle trajectories, where statistical averages are obtained from many realizations of single-particle simulation. This is an idealized setting, which can be justified only for diluted particles (with near zero density) in a viscous fluid. In a realistic situation, for relatively large and dense particles, crowding and strong correlations in the motion of particle can arise due to the steric interactions among the particles, which can compromise the ability of the channel to separate particles in practical applications. To study the effects of crowding and interparticle correlations on the collective transport of particles in a periodic channel is important and warrants further investigation.

Another limitation of the present paper is that transport is assumed to occur in a 2D channel. In fact, the 2D channel illustrated in Fig. 1(a) can be regarded as a cross section of a more realistic 3D periodic channel in the  $x$  direction. The diffusive movements of particles are restricted by the channel boundaries in the  $y$  and  $z$  directions. The static and periodic driving forces applied on the particles are along the  $x$  direction. If these forces are reasonably strong so that the gravity of the particles can be neglected, the equations of motion the particles in the  $y$  and  $z$  directions are the same. This feature, coupled with the symmetry of the spherical channel geometry, stipulates that the average velocity of the particles in the 3D channel be the same as that in the 2D case. Using the Fick-Jacobs approximation to integrate out the  $y$  and  $z$  variables, the end result is an effective 1D description based on the Fick-Jacobs equation. Under those circumstances, significant deviations in the diffusion dynamics in 3D from those in 2D are not expected.

## ACKNOWLEDGMENTS

We thank Yongge Li and Ruoxing Mei for helpful discussions. This work was supported by the National Natural Science Foundation of China under Grants No. 11972292 and No. 11672233, by the 111 Project under Grant No. BP0719007, and by the Innovation Foundation for Doctor Dissertation of Northwestern Polytechnical University under Grant No. CX201925. Y.C.L. was supported by the Office of Naval Research under Grant No. N00014-21-1-2323.

## APPENDIX: DERIVATION OF EQ. (13)

The mean velocity is a key quantity characterizing the transport efficiency of particles through a confined space, which can be analytically derived through the mean first passage time [38–40], the average time required for a stochastic process  $x(t)$  to reach the boundary or leave a specific area for the first time. At the initial time  $t_0$ , the particle position in the  $x$  direction is  $x_0$ . Since the confined space is a periodic channel of spatial period  $L$ , the barriers across which the particles move from one compartment to an adjacent one in the channel

are identical. It suffices to calculate the first passage time in a unit cell of length  $L$ , which is a random variable denoted as  $t(x_0 \rightarrow x_0 + L)$ . The particle current is

$$J = \frac{L}{\langle T_1(x_0 \rightarrow x_0 + L) \rangle}, \tag{A1}$$

where  $\langle \cdot \rangle$  denotes the mean first passage time. The  $n$ th moment of the first passage time is

$$T_n(x_0 \rightarrow x_0 + L) := \langle t^n(x_0 \rightarrow x_0 + L) \rangle, \tag{A2}$$

where  $T_0(x_0 \rightarrow x_0 + L) = 1$  and  $T_1(x_0 \rightarrow x_0 + L)$  is the mean first passage time. We have

$$J = \frac{L}{T_1(x_0 \rightarrow x_0 + L)}. \tag{A3}$$

To derive an analytic formula for  $J$ , we use the Fokker-Plank operator  $\Gamma$  defined as

$$\Gamma = \frac{\partial}{\partial x} \left[ D(x)e^{-V(x)} \frac{\partial}{\partial x} e^{V(x)} \right]. \tag{A4}$$

$$T_1 = \int_0^{+\infty} t w(t) dt = - \int_0^{+\infty} \int_{x_0}^{x_0+L} t \frac{\partial P(x, t)}{\partial t} dx dt = - \int_{x_0}^{x_0+L} \int_0^{+\infty} t \frac{\partial P(x, t)}{\partial t} dt dx. \tag{A9}$$

Carrying out the partial integration, we get

$$T_1 = \int_{x_0}^{x_0+L} \int_0^{+\infty} P(x, t) dt dx. \tag{A10}$$

Applying the backward operator  $\Gamma^+$  to Eq. (A10), we get

$$\Gamma^+ T_1 = e^{V(x)} \frac{\partial}{\partial x} \left[ D(x)e^{-V(x)} \frac{\partial}{\partial x} \right] T_1 = -1 \tag{A11}$$

or

$$\frac{\partial}{\partial x} \left[ D(x)e^{-V(x)} \frac{\partial}{\partial x} \right] T_1 = -e^{-V(x)}. \tag{A12}$$

Through integration, we get

$$\frac{\partial}{\partial x} T_1 = \frac{e^{V(x)}}{D(x)} \left[ - \int_a^x e^{-V(z)} dz + K_1 \right], \tag{A13}$$

where  $a$  is an arbitrary point in the given domain and  $K_1$  is an integration constant. Imposing the reflecting boundary condition at  $x \rightarrow -\infty$ :

$$\frac{\partial T_1}{\partial x} \Big|_{x=-\infty} = 0, \tag{A14}$$

we obtain

$$K_1 = \int_a^{-\infty} e^{-V(z)} dz. \tag{A15}$$

Substituting Eq. (A15) into Eq. (A13), we get

$$\frac{\partial}{\partial x} T_1 = - \frac{e^{V(x)}}{D(x)} \int_{-\infty}^x e^{-V(z)} dz, \tag{A16}$$

Using  $\Gamma$  in the Fick-Jacobs equation [Eq. (9)] in the main text, we get

$$\frac{\partial P(x, t)}{\partial t} = \Gamma P(x, t), \tag{A5}$$

The corresponding backward operator  $\Gamma^+$ , which is the adjoint operator of  $\Gamma$ , is given by

$$\Gamma^+ = e^{V(x)} \frac{\partial}{\partial x} \left[ D(x)e^{-V(x)} \frac{\partial}{\partial x} \right]. \tag{A6}$$

The probability function  $W(t)$  of a realization that starts from  $x_0$  and has not reached the absorbing boundary  $x_0 + L$  at time  $t$  is

$$W(t) = \int_{x_0}^{x_0+L} P(x, t) dx. \tag{A7}$$

The probability distribution function  $w(t)$  for the first passage time  $t$  is then given by

$$w(t) = - \frac{dW(t)}{dt} = - \int_{x_0}^{x_0+L} \frac{\partial P(x, t)}{\partial t} dx. \tag{A8}$$

The mean first passage time  $T_1(x_0 \rightarrow x_0 + L)$  is the first moment of  $t(x_0 \rightarrow x_0 + L)$ . We have

so

$$T_1 = - \int_b^x \frac{e^{V(y)}}{D(y)} dy \int_{-\infty}^y e^{-V(z)} dz + K_2, \tag{A17}$$

where  $b$  is an arbitrary point in the given domain and  $K_2$  is second integration constant. With the absorbing boundary condition at  $x = x_0 + L$ :  $T_1(x_0 + L) = 0$ , we get

$$K_2 = \int_b^{x_0+L} \frac{e^{V(y)}}{D(y)} dy \int_{-\infty}^y e^{-V(z)} dz. \tag{A18}$$

Substituting  $K_2$  back into Eq. (A17) leads to

$$T_1(x \rightarrow x + L) = \int_x^{x_0+L} \frac{e^{V(y)}}{D(y)} dy \int_{-\infty}^y e^{-V(z)} dz. \tag{A19}$$

The final equation for the first moment of the first passage time from a fixed point  $x_0$  to  $x_0 + L$  is

$$T_1(x_0 \rightarrow x_0 + L) = \int_{x_0}^{x_0+L} \frac{e^{V(x)}}{D_s(x)} dx \int_{-\infty}^x e^{-V(y)} dy. \tag{A20}$$

For clarity, we write

$$T_1(x_0 \rightarrow x_0 + L) = \int_{x_0}^{x_0+L} \tilde{I}(x) dx, \tag{A21}$$

where  $I(x)$  is given by

$$\tilde{I}(x) = \frac{e^{V(x)}}{D(x)} \int_{-\infty}^x e^{-V(y)} dy. \tag{A22}$$

Because the restricted channel is periodic and has a mirror symmetry, we have  $w_{e^+}(x) = -w_{e^-}(x)$  and

$w_{e+}(x + L) = w_{e+}(x)$ . In addition,  $D(x)$  is periodic [Eq. (11)]:  $D(x + L) = D(x)$ . From Eq. (10), we can write the free energy as

$$\begin{aligned} V(x) &= U(x) - TS(x) \\ &= -(f_1 + f_0)(r_p/a)x - \ln [2w_{e+}(x)] \text{ with} \\ U(x) &= -(f_1 + f_0)(r_p/a)x, \end{aligned}$$

which give

$$\begin{aligned} V(x + L) &= V(x) + [-(f_1 + f_0)(r_p/a)]L, \\ U(x + L) &= U(x) + [-(f_1 + f_0)(r_p/a)]L, \end{aligned}$$

where we have assumed that the force on the particle is  $f_1 + f_0$  with  $f_1$  being static and  $f_0$  being controllable. Using

$$\begin{aligned} \int_{-\infty}^x e^{-V(y)} dy &= \int_{-\infty}^x e^{-[U(y) - TS(y)]} dy \\ &= \sum_{m=0}^{\infty} \int_{x-L}^x e^{-V(y)} e^{[-(f_1+f_0)(r_p/a)]Lm} dy \\ &= \frac{1}{1 - e^{[-(f_1+f_0)(r_p/a)]L}} \int_{x-L}^x e^{-V(y)} dy, \end{aligned} \tag{A23}$$

we can simplify  $\tilde{I}(x)$  as

$$\tilde{I}(x) = \frac{e^{V(x)}}{D(x)(1 - e^{[-(f_1+f_0)(r_p/a)]L})} \int_{x-L}^x e^{-V(y)} dy. \tag{A24}$$

The mean first passage time  $T_1(x_0 \rightarrow x_0 + L)$  is given by

$$T_1(x_0 \rightarrow x_0 + L) = \frac{1}{1 - e^{[-(f_1+f_0)(r_p/a)]L}} \int_{x_0}^{x_0+L} \frac{e^{V(x)}}{D(x)} dx \int_{x-L}^x e^{-V(y)} dy. \tag{A25}$$

Accordingly, the particle current  $J(f_0)$  is given by

$$J(f_0) = \frac{L}{T_1(x_0 \rightarrow x_0 + L)} = \frac{L(1 - e^{[-(f_1+f_0)(r_p/a)]L})}{\int_{x_0}^{x_0+L} \frac{e^{V(x)}}{D(x)} dx \int_{x-L}^x e^{-V(y)} dy}. \tag{A26}$$

Since the initial position  $x_0$  is arbitrary, we set  $x_0 = 0$ . In addition, we have  $L = 1$ . These lead to Eq. (13). Note that the force exerted on the diffusion particles is time periodic. The average velocity of Brownian particles can be obtained by averaging over a single period, which is

$$\langle v \rangle = \frac{1}{\tau} \int_0^{\tau} J(F(t)) dt = \frac{1}{2}(J_1 + J_2), \tag{A27}$$

where

$$J_1 = (1 - \varepsilon)J\left(\frac{1 + \varepsilon}{1 - \varepsilon}f_0\right) \text{ and } J_2 = (1 + \varepsilon)J(-f_0). \tag{A28}$$

---

[1] P. Magaretti, I. Pagonabarraga, and M. Rubi, Entropic transport in confined media: A challenge for computational studies in biological and soft-matter systems, *Front. Phys.* **1**, 21 (2013).  
 [2] S. M. Bezrukov, L. Schimansky-Geier, and G. Schmid, Brownian motion in confined geometries, *Eur. Phys. J.: Spec. Top.* **223**, 3021 (2014).  
 [3] S. Pagliara, S. L. Dettmer, K. Misiunas, L. Lea, Y. Tan, and U. F. Keyser, Diffusion coefficients and particle transport in synthetic membrane channels, *Eur. Phys. J.: Spec. Top.* **223**, 3145 (2014).  
 [4] K. J. Krause, K. Mathwig, B. Wolfrum, and S. G. Lemay, Brownian motion in electrochemical nanodevices, *Eur. Phys. J.: Spec. Top.* **223**, 3165 (2014).  
 [5] X. Ao, P. K. Ghosh, Y. Li, G. Schmid, P. Hänggi, and F. Marchesoni, Active Brownian motion in a narrow channel, *Eur. Phys. J.: Spec. Top.* **223**, 3227 (2014).  
 [6] E. Locatelli, F. Baldovin, E. Orlandini, and M. Pierno, Active Brownian particles escaping a channel in single file, *Phys. Rev. E* **91**, 022109 (2015).  
 [7] X. Bian, C. Kim, and G. E. Karniadakis, 111 years of Brownian motion, *Soft Matter* **12**, 6331 (2016).  
 [8] C. L. X. Yang and, Y.-Y. Li, F. Marchesoni, P. Hänggi, and H. P. Zhang, Hydrodynamic and entropic effects on colloidal diffusion in corrugated channels, *Proc. Nat. Acad. Sci. U.S.A.* **114**, 9564 (2017).  
 [9] O. Bénichou1, P. Illien, G. Oshanin, A. Sarracino, and R. Voituriez1, Tracer diffusion in crowded narrow channels, *J. Phys.: Condens. Matter* **30**, 443001 (2018).  
 [10] Z. Siwy and A. Fuliński, Fabrication of a Synthetic Nanopore Ion Pump, *Phys. Rev. Lett.* **89**, 198103 (2002).  
 [11] Z. Siwy, I. D. Kosińska, A. Fuliński, and C. R. Martin, Asymmetric Diffusion Through Synthetic Nanopores, *Phys. Rev. Lett.* **94**, 048102 (2005).  
 [12] I. D. Kosińska, I. Goychuk, M. Kostur, G. Schmid, and P. Hänggi, Rectification in synthetic conical nanopores: A one-dimensional Poisson-Nernst-Planck model, *Phys. Rev. E* **77**, 031131 (2008).

- [13] M. Barrer, R. *Zeolites and Clay Minerals as Sorbents and Molecular Sieves* (Academic Press, London, 1978).
- [14] C. Baerlocher, D. Olson, and W. Meier, *Atlas of Zeolite Framework Types* (Elsevier, Amsterdam, 2001).
- [15] B. Hille, *Ionic Channels of Excitable Membranes* (Sinauer Associates, Sunderland, 1992).
- [16] P. Gates, K. Cooper, J. Rae, and R. Eisenberg, Predictions of diffusion models for one-ion membrane channels, *Prog. Biophys. Mol. Biol.* **53**, 153 (1989).
- [17] R. A. Siegel, Theoretical analysis of inward hemispheric release above and below drug solubility, *J. Controlled Release* **69**, 109 (2000).
- [18] M. H. Jacobs, *Diffusion Process* (Springer, Berlin, 1967).
- [19] P. S. Burada, G. Schmid, and P. Hänggi, Entropic transport: A test bed for the Fick-Jacobs approximation, *Phil. Trans. R. Soc. A* **367**, 3157 (2009).
- [20] R. Zwanzig, Diffusion past an entropy barrier, *J. Phys. Chem.* **96**, 3926 (1992).
- [21] D. Reguera, J. M. Rubí, Kinetic equations for diffusion in the presence of entropic barriers, *Phys. Rev. E* **64**, 061106 (2001).
- [22] P. Kalinay and J. K. Percus, Extended Fick-Jacobs equation: Variational approach, *Phys. Rev. E* **72**, 061203 (2005).
- [23] P. Kalinay and J. K. Percus, Corrections to the Fick-Jacobs equation, *Phys. Rev. E* **74**, 041203 (2006).
- [24] P. S. Burada, G. Schmid, D. Reguera, J. M. Rubí, and P. Hänggi, Biased diffusion in confined media: Test of the Fick-Jacobs approximation and validity criteria, *Phys. Rev. E* **75**, 051111 (2007).
- [25] A. M. Berezhkovskii, M. A. Pustovoit, and S. M. Bezrukov, Diffusion in a tube of varying cross section: Numerical study of reduction to effective one-dimensional description, *J. Chem. Phys.* **126**, 134706 (2007).
- [26] D. Reguera and J. M. Rubi, Engineering tube shapes to control confined transport, *Euro. Phys. J. Spec. Top.* **223**, 3079 (2014).
- [27] Y. Li, Y. Xu, W. Xu, Z.-C. Deng, and J. Kurths, Fine separation of particles via the entropic splitter, *Phys. Rev. E* **96**, 022152 (2017).
- [28] Y. Li, Y. Xu, and J. Kurths, Roughness-enhanced transport in a tilted ratchet driven by Lévy noise, *Phys. Rev. E* **96**, 052121 (2017).
- [29] R. Mei, Y. Xu, and J. Kurths, Transport and escape in a deformable channel driven by fractional Gaussian noise, *Phys. Rev. E* **100**, 022114 (2019).
- [30] M. V. Vazquez, A. M. Berezhkovskii, and L. Dagdug, Diffusion in linear porous media with periodic entropy barriers: A tube formed by contacting spheres, *J. Chem. Phys.* **129**, 046101 (2008).
- [31] A. M. Berezhkovskii and L. Dagdug, Biased diffusion in tubes formed by spherical compartments, *J. Chem. Phys.* **133**, 134102 (2010).
- [32] A. M. Berezhkovskii and S. M. Bezrukov, On the applicability of entropy potentials in transport problems, *Eur. Phys. J.: Spec. Top.* **223**, 3063 (2014).
- [33] K. J. Huang, S. J. Qin, Z. C. Bai, X. Zhang, and J. D. Mai, Entropy-based separation of yeast cells using a microfluidic system of conjoined spheres, *J. Appl. Phys.* **114**, 194702 (2013).
- [34] K. D. Dorfman, D. Gupta, A. Jain, A. Muralidhar, and D. R. Tree, Hydrodynamics of DNA confined in nanoslits and nanochannels, *Eur. Phys. J.: Spec. Top.* **223**, 3179 (2014).
- [35] M. V. Fistul, Symmetry broken motion of a periodically driven Brownian particle: Nonadiabatic regime, *Phys. Rev. E* **65**, 046621 (2002).
- [36] P. Kalinay, Rectification of confined diffusion driven by a sinusoidal force, *Phys. Rev. E* **89**, 042123 (2014).
- [37] D. Reguera, G. Schmid, P. S. Burada, J. M. Rubí, P. Reimann, and P. Hänggi, Entropic Transport: Kinetics, Scaling, and Control Mechanisms, *Phys. Rev. Lett.* **96**, 130603 (2006).
- [38] P. Hänggi, P. Talkner, and M. Borkovec, Reaction-rate theory: Fifty years after Kramers, *Rev. Mod. Phys.* **62**, 251 (1990).
- [39] P. Reimann, C. Van den Broeck, H. Linke, P. Hänggi, J. M. Rubi, and A. Pérez-Madrid, Giant Acceleration of Free Diffusion by Use of Tilted Periodic Potentials, *Phys. Rev. Lett.* **87**, 010602 (2001).
- [40] P. Reimann, C. Van den Broeck, H. Linke, P. Hänggi, J. M. Rubi, and A. Pérez-Madrid, Diffusion in tilted periodic potentials: Enhancement, universality, and scaling, *Phys. Rev. E* **65**, 031104 (2002).
- [41] B.-Q. Ai, Transport of overdamped Brownian particles in a two-dimensional tube: Nonadiabatic regime, *Phys. Rev. E* **80**, 011113 (2009).
- [42] I. Pineda, M.-V. Vazquez, A. M. Berezhkovskii, and L. Dagdug, Diffusion in periodic two-dimensional channels formed by overlapping circles: Comparison of analytical and numerical results, *J. Chem. Phys.* **135**, 224101 (2011).
- [43] P. Kalinay, Mapping of forced diffusion in quasi-one-dimensional systems, *Phys. Rev. E* **80**, 031106 (2009).